

Measurement of open bottom hadron production via displaced J/ψ , D^0 and electrons in Au+Au collisions at $\sqrt{s_{NN}} = 200$ GeV at STAR

Xiaolong Chen (for the STAR Collaboration)*

State Key Laboratory of Particle Detection and Electronics

University of Science and Technology of China

E-mail: xlchen89@mail.ustc.edu.cn

Recent RHIC and LHC results show that the nuclear modification factor of D^0 mesons at high transverse momenta as well as their elliptic flow are similar to those of light flavor hadrons, indicating that charm quarks also interact very strongly with the Quark Gluon Plasma (QGP). During interactions, charm quarks lose substantial energy and gain significant elliptic flow. It is then imperative to measure bottom quark production in heavy-ion collisions in order to study the mass dependence of parton-medium interactions in the QGP. In these proceedings, measurements of open bottom hadron production obtained through reconstruction of their displaced decay daughters ($B \rightarrow J/\psi, D^0, e$) in Au+Au collisions at $\sqrt{s_{NN}} = 200$ GeV at STAR are presented. These measurements are made possible thanks to the high-precision vertexing and tracking provided by the Heavy Flavor Tracker. Nuclear modification factors of J/ψ , D^0 and electrons from open bottom hadron decays are measured and compared with those of open charm hadrons at RHIC.

*International Conference on Hard and Electromagnetic Probes of High-Energy Nuclear Collisions
30 September - 5 October 2018
Aix-Les-Bains, Savoie, France*

*Speaker.

1. Introduction

Heavy flavor quarks (c , b), due to their large masses, are predominantly produced through initial hard scatterings during high energy heavy-ion collisions. Thus they experience the entire evolution of the hot and dense medium created in the collisions. While interacting with the medium, heavy quarks lose energy. In particular, it is expected that bottom quarks lose less energy than charm quarks [1, 2, 3]. Systematic investigations of charm and bottom hadron production in heavy-ion collisions is crucial for understanding the parton energy loss mechanism in the medium. In these proceedings, we present the measurements of open bottom hadron production in Au+Au collisions at $\sqrt{s_{NN}} = 200$ GeV at STAR through three inclusive decay channels ($B \rightarrow J/\psi$, D^0 , e).

2. Measurements of bottom production at STAR

Mainly four STAR sub-detectors are used for measurements of bottom production. The Time Projection Chamber (TPC) is the main detector used for reconstruction of charged tracks and particle identification through energy loss (dE/dx) [4]. The Time of Flight detector (TOF) provides information about velocity ($1/\beta$) for particle identification [5] and the Barrel Electromagnetic Calorimeter (BEMC) is used to trigger on high p_T electrons and identify them through fraction of their deposited energy (p/E) [6]. The Heavy Flavor Tracker (HFT) provides an excellent pointing resolution of less than $30 \mu\text{m}$ for charged particles at momenta larger than $1.5 \text{ GeV}/c$ in both the beam direction and the transverse plane [7], which makes it possible for bottom measurements at STAR. These detectors cover full azimuth within $|\eta| < 1$.

2.1 $B \rightarrow J/\psi$

We use the pseudo-proper decay length $l_{J/\psi}$ distribution to extract the non-prompt J/ψ contribution (from B-decay) to the inclusive J/ψ yield. The pseudo-decay length is defined as $l_{J/\psi} = \frac{\vec{L} \cdot \hat{p}}{|\vec{p}|/c} M_{J/\psi}$, where \vec{L} is the vector from the primary vertex to the decay vertex of J/ψ , \vec{p} is the J/ψ momentum, \hat{p} is its unit vector, and $M_{J/\psi}$ is the J/ψ rest mass. Since bottom hadrons have a longer lifetime than J/ψ , the non-prompt J/ψ will have a wider and more positive $l_{J/\psi}$ distribution than the prompt ones.

The left panel of Figure 1 shows an example of template fitting of the $l_{J/\psi}$ distribution within $3 < p_T^{J/\psi} < 5 \text{ GeV}/c$ in 0-80% centrality. The black circles show the $l_{J/\psi}$ distribution of inclusive J/ψ after background subtraction. The templates for prompt J/ψ (blue line) and non-prompt J/ψ (red line) are obtained with a data-driven fast simulation, in which J/ψ and bottom hadron (B^0 , B^\pm) p_T spectra are generated from a FONLL calculation [8]. The non-prompt J/ψ fraction as a function of J/ψ p_T is extracted (red circles) and compared with the CEM+FONLL calculation for 200 GeV p+p collisions (grey band) [8, 9] in the central panel of Figure 1. The nuclear modification factor R_{AA} of non-prompt J/ψ is calculated with the following formula

$$R_{AA}^{B \rightarrow J/\psi} = \frac{f_{Au+Au}^{B \rightarrow J/\psi}(data)}{f_{p+p}^{B \rightarrow J/\psi}(theory)} R_{AA}^{inc. J/\psi}(data) \quad (2.1)$$

where $f_{Au+Au}^{B \rightarrow J/\psi}(data)$ is the measured fraction of non-prompt J/ψ in Au+Au collisions, $f_{p+p}^{B \rightarrow J/\psi}(theory)$ is the fraction in p+p collisions obtained from the CEM+FONLL calculation, and $R_{AA}^{inc. J/\psi}(data)$

is the R_{AA} of inclusive J/ψ measured by STAR [10]. The right panel of Figure 1 shows the R_{AA} of non-prompt J/ψ (red filled circles) and inclusive D^0 (blue open circles) [11] as a function of p_T in 0-80% centrality. A strong suppression for non-prompt J/ψ is observed at high p_T , which is similar to that of inclusive D^0 mesons.

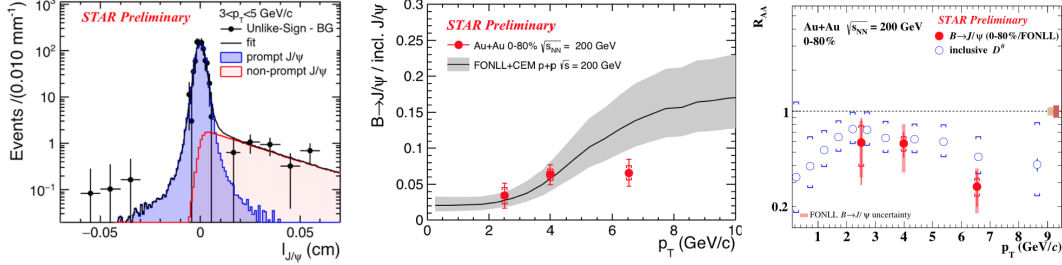


Figure 1: (Left) $l_{J/\psi}$ distribution within $3 < p_T^{J/\psi} < 5$ GeV/c in 0-80% centrality with fitted MC templates. (Middle) non-prompt J/ψ fraction as a function of J/ψ p_T in 0-80% centrality (red circles), compared with the FONLL+CEM calculation (grey band). (Right) non-prompt J/ψ R_{AA} (red circles) compared with inclusive D^0 R_{AA} (blue circles) as a function of p_T .

2.2 $B \rightarrow D^0$

The distribution of the three-dimensional distance of closest approach (DCA) of D^0 to the primary vertex is used to extract the non-prompt D^0 contribution (from B-decay) to the inclusive D^0 yield. The non-prompt D^0 DCA distribution is wider than prompt D^0 since bottom hadrons' lifetimes are longer compared to D^0 . The left panel of Figure 2 shows the extraction of non-prompt D^0 fraction within $3 < p_T^{D^0} < 5$ GeV/c in 0-80% centrality. The templates of prompt (blue line) and non-prompt (green line) D^0 are obtained from the data-driven fast simulation. After efficiency correction, the non-prompt D^0 fraction as a function of D^0 p_T is extracted (see the central panel of Figure 2) for three different centralities of Au+Au collisions at $\sqrt{s_{NN}} = 200$ GeV. No clear centrality dependence is observed within the precision of the data. The result is compared with the non-prompt D^0 fraction in p+p collisions at $\sqrt{s} = 200$ GeV. The latter is calculated using the non-prompt D^0 yield from FONLL prediction [8], and the inclusive D^0 yield either from FONLL prediction (green band) [8] or from the measurement at STAR (yellow band) [12]. With the p+p baseline of the non-prompt D^0 yield from FONLL prediction, the non-prompt D^0 R_{AA} can be calculated using the following formula

$$R_{AA}^{B \rightarrow D^0} = \frac{1}{\langle N_{coll} \rangle} \frac{f_{Au+Au}^{B \rightarrow D^0}(data) \times dN_{Au+Au}^{inc. D^0} / dp_T(data)}{dN_{p+p}^{B \rightarrow D^0} / dp_T(FONLL)} \quad (2.2)$$

where $f_{Au+Au}^{B \rightarrow D^0}(data)$ is the non-prompt D^0 fraction measured in Au+Au collisions, $dN_{Au+Au}^{inc. D^0} / dp_T(data)$ is the inclusive D^0 yield measured in Au+Au collisions [11], and $dN_{p+p}^{B \rightarrow D^0} / dp_T(FONLL)$ is the non-prompt D^0 yield in p+p collisions from FONLL prediction. The right panel of Figure 2 shows the R_{AA} of non-prompt D^0 (red filled circles) as a function of D^0 p_T in 0-20% centrality. A strong suppression of non-prompt D^0 is observed at high p_T . When compared with inclusive D^0 in 0-10% centrality (blue open circles) [11], a hint of less suppression for non-prompt D^0 is observed.

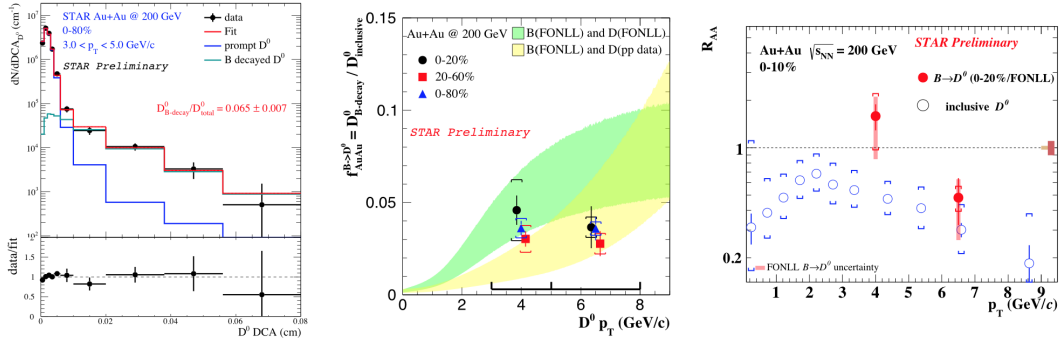


Figure 2: (Left) D^0 DCA distributions for $3 < p_T^{D^0} < 5$ GeV/c in 0-80% centrality with fitted MC templates. (Middle) non-prompt D^0 fraction as a function of $D^0 p_T$ in 0-20% (black circles), 20-60% (red squares) and 0-80% centrality (blue triangles), compared with the ratio of FONLL calculation for non-prompt D^0 to FONLL calculation for inclusive D^0 (green band) and to inclusive D^0 yield measurement in p+p collisions at $\sqrt{s} = 200$ GeV (yellow band). (Right) non-prompt $D^0 R_{AA}$ (red circles) compared with inclusive $D^0 R_{AA}$ (blue circles) as a function of $D^0 p_T$.

2.3 $B/D \rightarrow e$

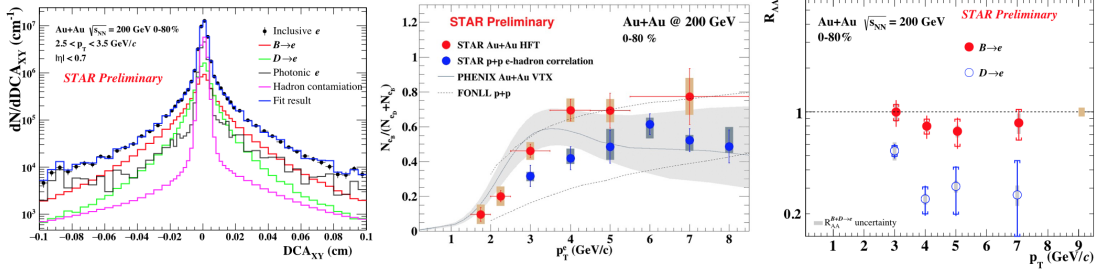


Figure 3: (Left) MC templates fitted to DCA_{XY} of inclusive electrons. (Middle) fraction of electrons from bottom hadron decays to the sum of those from charm and bottom hadron decays as a function of electron p_T (red circles) in Au+Au collisions at $\sqrt{s_{NN}} = 200$ GeV, compared with the measurement in p+p collisions (blue circles) and FONLL calculation (grey band). (Right) R_{AA} of electrons from decays of bottom (red circles) and charm (blue circles) hadrons as a function of electron p_T .

The electron DCA distribution in the transverse plane (DCA_{XY}) is used to extract the contribution of electrons originating from decays of charm and bottom hadrons to the inclusive electron yield. The left panel of Figure 3 shows the DCA_{XY} distribution of inclusive electrons with fitted MC templates of different contributions. The inclusive electron DCA_{XY} distribution (black circles) includes signals from Non-Photonic Electron (NPE, $B/D \rightarrow e$), as well as various background sources. The DCA_{XY} distributions from charm hadron decays (green line) and bottom hadron decays (red line) are obtained from simulations. The DCA_{XY} distributions of background electrons from gamma conversions and light meson Dalitz decays are obtained from real data at low- p_T region and from MC simulation at high- p_T region. Another background contribution comes from hadrons mis-identified as electrons. The central panel of Figure 3 shows the fraction of electrons from bottom hadron decays as a function of electron p_T in Au+Au collisions (red circles) and p+p

collisions [13]. These results (in p+p and Au+Au) are consistent with FONLL calculation in p+p collisions [8] and the measurement from PHENIX in Au+Au collisions [14], respectively. The right panel of Figure 3 shows the R_{AA} of electrons from bottom and charm hadron decays separately as a function of electron p_T in 0-80% centrality, which is calculated as

$$R_{AA}^{B \rightarrow e} = \frac{f_{Au+Au}^{B \rightarrow e}(data)}{f_{p+p}^{B \rightarrow e}(data)} R_{AA}^{NPE}(data), \quad R_{AA}^{D \rightarrow e} = \frac{1 - f_{Au+Au}^{B \rightarrow e}(data)}{1 - f_{p+p}^{B \rightarrow e}(data)} R_{AA}^{NPE}(data) \quad (2.3)$$

where $f_{Au+Au}^{B \rightarrow e}(data)$ and $f_{p+p}^{B \rightarrow e}(data)$ are fractions of $B \rightarrow e$ in Au+Au collisions and p+p collisions, and $R_{AA}^{NPE}(data)$ is the R_{AA} of NPE [15]. Less suppression for $B \rightarrow e$ compared to $D \rightarrow e$ is observed on a level of $\sim 2\sigma$ significance which is consistent with the mass hierarchy of parton energy loss.

3. Summary and Outlook

In summary, we report on the STAR measurements of open bottom hadron production obtained by identifying their decays into displaced J/ψ , D^0 and electrons in Au+Au collisions at $\sqrt{s_{NN}} = 200$ GeV. Strong suppressions for $B \rightarrow J/\psi$ and $B \rightarrow D^0$ at high p_T are observed. The production of $B \rightarrow e$ is less suppressed than that of $D \rightarrow e$ with a significance level of about 2σ . Approximately 1.5 times more minimum-bias and 5 times more high p_T triggered events were recorded in year 2016 by STAR which are going to be analyzed to further improve the precision of the open bottom measurements in $B \rightarrow D^0$ and $B \rightarrow e$ channels.

Acknowledgments: This work was supported partially by the National Natural Science Foundation of China (No. 11890712), the Youth Innovation Promotion Association Fund of CAS (No. CX2030040079), and the Science and Technological Fund of Anhui Province for Outstanding Youth (No. 1808085J02).

References

- [1] R. Baier, D. Schiff and B. Zakharov, *Ann. Rev. Nucl. Part. Sci.* **50** (2000) 37 [hep-ph/0002198].
- [2] M. Gyulassy et al., *Quark-Gluon Plasma 3*, pp. 123-191. World Scientific, 2004 [nucl-th/0302077].
- [3] A. Buzzatti and M. Gyulassy, *Phys. Rev. Lett.* **108** (2012) 022301 [arXiv:1106.3061].
- [4] M. Anderson et al., *Nucl. Instrum. Meth. A* **499** (2003) 659 [nucl-ex/0301015].
- [5] B. Bonner et al., *Nucl. Instrum. Meth. A* **508** (2003) 181.
- [6] M. Beddo et al., *Nucl. Instrum. Meth. A* **499** (2003) 725.
- [7] G. Contin et al., *Nucl. Instrum. Meth. A* **907** (2018) 60 [arXiv:1710.02176].
- [8] M. Cacciari, P. Nason and R. Vogt, *Phys. Rev. Lett.* **95** (2005) 122001.
- [9] A. D. Frawley, T. Ullrich and R. Vogt, *Phys. Rept.* **462** (2008) 125 [arXiv:0806.1013].
- [10] T. Todoroki, *J. Phys. Conf. Ser.* vol. 779, p. 012040, IOP Publishing, 2017 [arXiv:1612.02499].
- [11] G. Xie, *Measurements of open charm hadron production in Au+Au collisions at s = 200 GeV at STAR*, this conference.
- [12] L. Adamczyk et al., *Phys. Rev. D* **86** (2012) 072013 [arXiv:1204.4244].
- [13] M. Aggarwal et al., *Phys. Rev. Lett.* **105** (2010) 202301 [arXiv:1007.1200].
- [14] A. Adare et al., *Phys. Rev. C* **93** (2016) 034904 [arXiv:1509.04662].
- [15] S. Zhang, *Int. J. Mod. Phys. Conf. Ser.* vol. 46, p. 1860014, World Scientific, 2018.